Int J Mech Mater Des (2023) 19:817–830
https://doi.org/10.1007/s10999-023-09660-x

A size-dependent effect of smart functionally graded piezoelectric porous nanoscale plates

Lieu B. Nguyen · H. Nguyen-Xuan · Chien H. Thai · P. Phung-Van

Received: 6 April 2023 / Accepted: 25 April 2023 / Published online: 29 May 2023

Abstract This paper presents a size-dependent isogeometric analysis of smart functionally graded porous nanoscale plates made of two piezoelectric materials. Two porous distributions, namely even and uneven, are considered along the thickness direction. To take into account for size-dependent effects, the nonlocal elasticity theory proposed by Eringen is employed to investigate the behaviors of the smart nanoplate. An electric potential field is adopted based on the Maxwell's equation. The governing equations for smart functionally graded piezoelectric porous nanoplates are obtained and utilized by a combination of higher-order shear deformation theory and non-uniform rational B-splines formulations. The present approximation is capable of meeting the necessary conditions with at least third-order derivatives in the approximate formulations of the smart nanoplate. The natural frequencies of the smart nanoplate are fully investigated by studying the influences of power-law index, external electric voltage, porosity coefficient, boundary condition, porosity distributions, and nonlocal parameter, respectively. The present results, when compared to those from published documents, have been evaluated and found to be both reliable and effective. This paper reports several new computational results that can be of great interest to researchers due to the innovative approach and both the development and future application for smart nanostructures.

Keywords Isogeometric approach · Smart functionally graded piezoelectric porous nanoplates · A small-scale effect · Electro-mechanical materials · Porosity

L. B. Nguyen
Faculty of Civil Engineering, Ho Chi Minh City University of Technology and Education, Ho Chi Minh City, Vietnam

H. Nguyen-Xuan
CIRTECH Institute, HUTECH University, Ho Chi Minh City, Vietnam

C. H. Thai (✉)
Division of Computational Mechanics, Institute for Computational Science, Ton Duc Thang University, Ho Chi Minh City, Vietnam
e-mail: thaihoangchien@tdtu.edu.vn

C. H. Thai
Faculty of Civil Engineering, Ton Duc Thang University, Ho Chi Minh City, Vietnam

P. Phung-Van (✉)
Faculty of Civil Engineering, HUTECH University, Ho Chi Minh City, Vietnam
e-mail: pv.phuc86@hutech.edu.vn

1 Introduction

Piezoelectric materials have been of great interest due to their exceptional electro-mechanical coupling characteristics. Functionally graded piezoelectric materials (FGPMs) have been developed to address the high stress concentration in the inner layer of piezoelectric

materials and prevent corrosion between bonding layers. In recent years, there has been a growing interest in studying the behavior of FGPMs in micro/nanostructures, which are widely used in structural health monitoring, active vibration control, and electromechanical systems.

Several studies have investigated the behavior of FGPM porous nanoplates using analytical and numerical methods. Kiani et al. (2011) performed the thermo-electrical buckling of piezoelectric FG material Timoshenko beams, while Nguyen et al. (2019) reported on the vibration analysis of functionally graded piezoelectric material porous plates using the C0-type higher-order shear deformation theory (C0-HSDT). Joubaneh et al. (2015) analyzed the thermal buckling of a solid circular plate made of porous material with piezoelectric sensor-actuator patches on its boundary, and Su et al. (2018) reported an exact solution for the electro-mechanical vibration properties of FG piezoelectric plates with their overall boundary. Behjat et al. (2009) studied the static bending, free vibration, and dynamic behavior of FG piezoelectric panels using finite element analysis under various loading types, while Zhang et al. (2008) reported analytical solutions for investigating the behavior of FG piezoelectric cylindrical actuators under a harmonic electric field using elastic membrane and shell theory. The dynamic control of smart piezoelectric composite plates was presented in the publications (Phung-Van et al. 2017a, 2017b) while the static analysis of FGPM structures was investigated in the references (Brischetto and Carrera 2009;). Chen et al. (2002; 2002) analyzed the free vibration of FGPM rectangle-shaped plates and hollow spheres using the laminated approximation approach together with state space formulations.

Owing to the rapid development of nano technique, small-scale effects are very attractive to researchers. Because the nanostructures made of FGMs/piezoelectric materials are usually employed in structural health monitoring, active vibration control and electromechanical systems, the mechanical analysis of FGM/piezoelectric nanostructures (Phung-Van et al. 2020a,b) has been rapidly developed. The thermo-electrical buckling properties of FG piezoelectric Timoshenko nanobeams under in-plane thermal loading and applied electric voltage were investigated by Ebrahimi and Salari (2015) using a Navier type solution and elasticity theory of Eringen. Zenkour and Aljadani (2019b) analyzed the thermo-electrical buckling of the FG piezoelectric nanoscale plate based on the refined hyperbolic higher-order shear deformation theory (HSDT) and Eringen's nonlocal theory. They also developed an analytical method for analysis of the thermal buckling of the actuated FG piezoelectric porous nanoplates (Zenkour and Aljadani 2019a). The nonlinear formulation of the FG piezoelectric material nanobeams was established by employing the Euler–Bernoulli model and the consistent size-dependent theory (Tadi 2016). Ebrahimi and Barati (2017) conducted an analytical study on the buckling behavior of higher-order shear deformable nanobeams made of FG piezoelectric materials implanted in an elastic foundation. Based on the novel modified couple stress theory and analytical solutions, Mehralian et al. (2016) proposed the size-dependent formulation of shear deformable FG piezoelectric cylindrical nanoshells. Li and Xiao (2021) performed the free vibration of a one-dimensional piezoelectric quasicrystal microbeam using the modified couple stress theory and differential quadrature technique.

The majority of previous research on FGPM structures has been based on analytical methods, with only a few studies focusing on micro/nanostructures. As we've known, to solving complex structures in engineering practices, numerical solutions are usually considered as the best candidate to use. This literature gap has prompted researchers to develop an effective numerical solution to analyze nanoplates integrated with piezoelectric materials. For calculating nanoplates, it always requires higher-order derivatives in governing equations. Recently, an effective numerical method, isogeometric analysis (IGA), which has shown several advanced properties, was firstly proposed by Hughes et al. (2005). Non-uniform rational B-spline (NURBS) basis functions are employed by IGA to accurately depict the geometry of structures and estimate the solution fields. One of its significant advantages is its ability to achieve any degree of smoothness by selecting the interpolation order, while lower continuity can be easily achieved through knot insertion. IGA has been effectively employed in various fields such as nanoplates (Phung-Van and Thai 2021; Phung-Van et al. 2021) and microplates (Thai 2020; Hung et al 2022), but its implementation to smart nanoplates is still restricted. Furthermore, the area of research concerning the size-dependent behavior of smart functionally graded piezoelectric nanoplates with porosity has not been thoroughly investigated. This paper aims

to address this research gap by proposing an effective numerical approach for conducting such an analysis. The findings of this paper are expected to be of great interest to researchers due to the innovative approach and the potential implications of the results.

2 Functionally graded piezoelectric porous materials

We now consider a functionally graded piezoelectric porous nanoplate (length a, width b, thickness h) under an electric field, as displayed in Fig. 1. In the FGPP, two piezoelectric materials consist of PZT-4 and PZT-5H to be mixed. Through the thickness direction, two porous distributions comprising of (i) even: positions of porosity are randomly distributed in the cross section (FGPP-I) and (ii) uneven: porosity is arranged around middle zone of the cross section (FGPP-II) are considered.

Based on the modified power law function scheme, the type of FGPP-I is expressed as

$$P(z) = P_t + \left(P_b - P_t\right)\left(\frac{z}{h} + \frac{1}{2}\right)^n - \frac{\alpha}{2}\left(P_b + P_t\right) \quad (1)$$

where P are the effective properties of the material, which include the elastic constants, piezoelectric constants, and dielectric constants; b and t represent the bottom and top surfaces of the plate, respectively; α is the porosity parameter which defines by $0<\alpha<1$ and n is the power index factor.

For the FGPP-II, the effective material property is defined as

$$P(z) = P_t + \left(P_b - P_t\right)\left(\frac{z}{h} + \frac{1}{2}\right)^n - \frac{\alpha}{2}\left(P_b + P_t\right)\left(1 - \frac{2|z|}{h}\right) \quad (2)$$

3 Mathematical formulations

3.1 Nonlocal Eringen's theory

A nanoplate subjected to an external body force (f_i) is considered in this research. The governing equations for a homogeneous anisotropic linearly piezoelectric material can be expressed as follows

$$\begin{aligned} &\overline{\sigma}_{ij,j} + f_i = \rho \ddot{u}_i \text{ in } V \\ &\overline{D}_{i,i} = 0 \text{ in } V \end{aligned} \quad (3)$$

where $\overline{\sigma}_{ij}$ is the nonlocal stress $\ddot{u}_i$ is the acceleration field; ρ is the density mass; $\overline{D}_i$ is the nonlocal electric potential and V is the volume.

Constitutive relations for the mechanical–electrical coupling of the FGPP nanoplates are given as

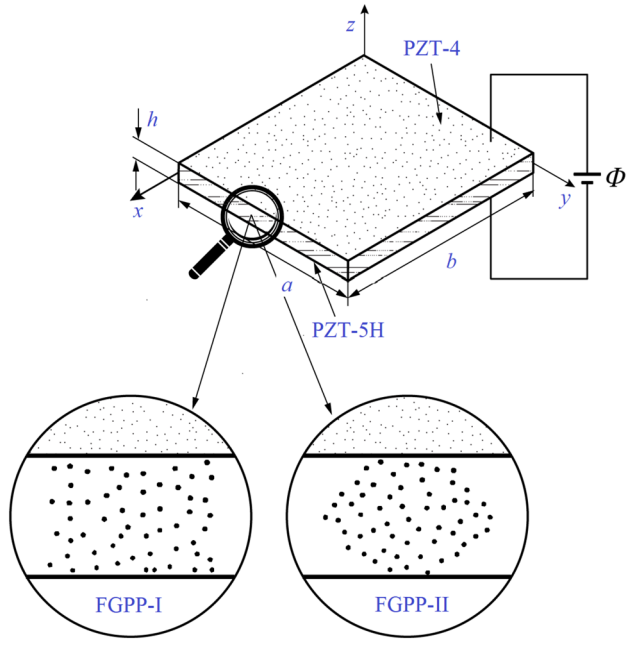

Fig. 1 Geometry of FGPP nanoplate

$$\begin{aligned}\sigma_{ij} &= C_{ijkl}\varepsilon_{kl} - e_{ijk}E_k \\ D_i &= e_{ijk}\varepsilon_{kl} + k_{ik}E_k\end{aligned} \tag{4}$$

where σ_{ij} and D_i are the local stress and local electric displacement, respectively; ε_{kl} and E_k indicate the local strain and electric field components, respectively; C_{ijkl},e_{ijk} and k_{ik} are respectively the elastic, piezoelectric and dielectric constants.

According to the nonlocal law suggested by Eringen, the nonlocal stress $\overline{\sigma}_{ij}$ and nonlocal electric displacement $\overline{D}_i$ can be defined as

$$\begin{aligned}\overline{\sigma}_{ij} &= \int_V \varsigma\left(|\mathbf{x}' - \mathbf{x}|, \tau\right)\sigma_{ij}\mathrm{d}\mathbf{x}' \\ \overline{D}_i &= \int_V \varsigma\left(|\mathbf{x}' - \mathbf{x}|, \tau\right)D_i\mathrm{d}\mathbf{x}'\end{aligned} \tag{5}$$

where $\mathbf{x}$ is a point in the body;$\mathbf{x}'$ is a neighbor point of $\mathbf{x}$; the kernel function $\varsigma\left(|\mathbf{x}' - \mathbf{x}|, \tau\right)$ indicates the nonlocal modulus; τ indicates a material constant; $|\mathbf{x}' - \mathbf{x}|$ is the distance.

By applied the differential operator $\left(1 - \lambda\nabla^2\right)$ for Eq. (5), it can be rewritten as (Lu et al. 2007)

$$\begin{aligned}&\left(1 - \lambda\nabla^2\right)\overline{\sigma}_{ij} = \sigma_{ij}\ , \quad \left(1 - \lambda\nabla^2\right)\overline{\sigma}_{ij,j} = \sigma_{ij,j} \\ &\left(1 - \lambda\nabla^2\right)\overline{D}_i = D_i\ , \quad \left(1 - \lambda\nabla^2\right)\overline{D}_{i,i} = D_{i,i}\end{aligned} \tag{6}$$

where λ is the nonlocal parameter. Similarly, we can be also used the above differential operator for Eq. (3). It can be formulated as

$$\begin{aligned}&\left(1 - \lambda\nabla^2\right)\overline{\sigma}_{ij,j} + \left(1 - \lambda\nabla^2\right)f_i = \left(1 - \lambda\nabla^2\right)\rho\ddot{u}_i \\ &\left(1 - \lambda\nabla^2\right)\overline{D}_{i,i} = 0\end{aligned} \tag{7}$$

Substituting Eq. (6) into Eq. (7) to attain Eq. (8):

$$\begin{aligned}&\sigma_{ij,j} + \left(1 - \lambda\nabla^2\right)f_i = \left(1 - \lambda\nabla^2\right)\rho\ddot{u}_i \\ &D_{i,i} = 0\end{aligned} \tag{8}$$

Applying the principle of virtual displacement and virtual electric potential, the integration form of Eq. (8) is expressed by

$$\begin{aligned}&\int_V \sigma_{ij,j}\delta u_i\mathrm{d}V + \int_V D_{i,i}\delta\Phi_i\mathrm{d}V + \left(1 - \lambda\nabla^2\right)f_i\delta u_i \\ &= \int_V \left(1 - \lambda\nabla^2\right)\rho\ddot{u}_i\delta u_i\mathrm{d}V\end{aligned} \tag{9}$$

where δu_i, $\delta\Phi_i$ are the virtual displacement vector and the virtual electric potential vector, respectively.

Applying the integration by parts and divergence theorem for the left-hand side of Eq. (9), it can be represented by

$$\begin{aligned}\int_V \sigma_{ij,j}\delta u_i\mathrm{d}V &= -\int_V \sigma_{ij}\delta u_{i,j}\mathrm{d}V + \int_{\Gamma_g} \sigma_{ij}n_i\delta u_i\mathrm{d}\Gamma_g \\ \int_V D_{i,i}\delta\Phi_i\mathrm{d}V &= -\int_V D_i\delta\Phi_{i,i}\mathrm{d}V + \int_{\Gamma_g} D_in_i\delta\Phi_i\mathrm{d}\Gamma_g\end{aligned} \tag{10}$$

where Γ_g is the Neumann boundary.

Substituting Eq. (10) into Eq. (9) and ignoring the integrated components on the boundary Γ_g, the final integration form of equilibrium equation is formulated as

$$\begin{aligned}&\int_V \sigma_{ij}\delta u_{i,j}\mathrm{d}V + \int_V D_i\delta\Phi_{,i}\mathrm{d}V + \int_V \left(1 - \lambda\nabla^2\right)\rho\ddot{u}_i\delta u_i\mathrm{d}V \\ &= \int_V \left(1 - \lambda\nabla^2\right)f_i\delta u_i\mathrm{d}V\end{aligned} \tag{11}$$

By replacing $\delta u_{i,j} = \delta\varepsilon_{ij}$ and $\delta\Phi_{,i} = -\delta\mathrm{E}_i$, Eq. (11) is rewritten as

$$\begin{aligned}&\int_V \delta\left(\varepsilon_{ij}\right)^T\sigma_{ij}\mathrm{d}V - \int_V \delta\left(E_i\right)^T D_i\mathrm{d}V + \int_V \left(1 - \lambda\nabla^2\right)\rho\delta\left(u_i\right)^T\ddot{u}_i\mathrm{d}V \\ &= \int_V \left(1 - \lambda\nabla^2\right)\delta\left(u_i\right)^T f_i\mathrm{d}V\end{aligned} \tag{12}$$

For the easy representation, Eq. (12) can be expressed by

$$\delta U + \delta K - \delta W = 0 \tag{13}$$

where

$$\begin{aligned}\delta U &= \int_V \delta\left(\varepsilon_{ij}\right)^T\sigma_{ij}\mathrm{d}V - \int_V \delta\left(\mathrm{E}_i\right)^T D_i\mathrm{d}V \\ \delta K &= \int_V \left(1 - \lambda\nabla^2\right)\delta\left(u_i\right)^T\rho\ddot{u}_i\mathrm{d}V \\ \delta W &= \int_V \left(1 - \lambda\nabla^2\right)\delta\left(u_i\right)^T f_i\mathrm{d}V\end{aligned} \tag{14}$$

in which δU, δK and δW represent the virtual strain energy, virtual kinetic energy, and virtual external work, respectively.

3.2 Displacement field

Through the generalized higher-order shear deformation theory, the displacement field is defined

$$\begin{aligned} u(x,y,z) &= u_0(x,y) - z\frac{\partial w(x,y)}{\partial x} + f(z)\beta_x(x,y) \\ v(x,y,z) &= v_0(x,y) - z\frac{\partial w(x,y)}{\partial y} + f(z)\beta_y(x,y) \\ w(x,y,z) &= w_0(x,y) \end{aligned} \tag{15}$$

where u_0,v_0,w,β_x and β_y are variables of displacement; $f(z) = z - 4z^3/3h^2$ is a continuous function.

Strain components can be displayed as

$$\boldsymbol{\varepsilon}^b = \left\{ \varepsilon_{xx} \;\; \varepsilon_{yy} \;\; \gamma_{xy} \right\}^{\mathrm{T}} = \boldsymbol{\varepsilon}_1 + z\boldsymbol{\varepsilon}_2 + f(z)\boldsymbol{\varepsilon}_3$$
$$\boldsymbol{\gamma} = \left\{ \gamma_{xz} \;\; \gamma_{yz} \right\}^{\mathrm{T}} = f'(z)\boldsymbol{\varepsilon}_s \tag{16}$$

where $f'(z)$ is the derivative of the function $f(z)$ and

$$\boldsymbol{\varepsilon}_1 = \begin{bmatrix} u_{0,x} \\ v_{0,y} \\ u_{0,y} + v_{0,x} \end{bmatrix};\; \boldsymbol{\varepsilon}_2 = -\begin{bmatrix} w_{0,xx} \\ w_{0,yy} \\ 2w_{0,xy} \end{bmatrix}$$
$$\boldsymbol{\varepsilon}_3 = \begin{bmatrix} \beta_{x,x} \\ \beta_{y,y} \\ \beta_{x,y} + \beta_{y,x} \end{bmatrix};\; \boldsymbol{\varepsilon}_s = \begin{bmatrix} \beta_x \\ \beta_y \end{bmatrix} \tag{17}$$

The FGPP nanoplate is performed under an initial electric voltage V_0 on the top and bottom surfaces. According to the Maxwell's formula, the electric potential is given as

$$\Phi(x,y,z) = g(z)\phi(x,y) + \frac{2z}{h}V_0 \tag{18}$$

where $\phi(x,y)$ is the electric potential; $g(z) = -\cos\left(\frac{\pi z}{h}\right)$. The electric fields are defined as

$$\begin{aligned} E_x &= -\Phi_{,x} = -g(z)\phi_{,x} \\ E_y &= -\Phi_{,y} = -g(z)\phi_{,y} \\ E_z &= -\Phi_{,z} = -g'(z)\phi - \frac{2V_0}{h} \end{aligned} \tag{19}$$

For easy numerical computations, the local stress and local electric displacement in Eq. (12) can be rewritten by an explicit form as

$$\begin{aligned} &\underbrace{\begin{Bmatrix} \sigma_{xx} \\ \sigma_{yy} \\ \sigma_{xy} \end{Bmatrix}}_{\boldsymbol{\sigma}^b} = \underbrace{\begin{bmatrix} \tilde{C}_{11} & \tilde{C}_{12} & 0 \\ \tilde{C}_{12} & \tilde{C}_{22} & 0 \\ 0 & 0 & \tilde{C}_{66} \end{bmatrix}}_{\mathbf{C}^b} \underbrace{\begin{Bmatrix} \varepsilon_{xx} \\ \varepsilon_{yy} \\ \varepsilon_{xy} \end{Bmatrix}}_{\boldsymbol{\varepsilon}^b} - \underbrace{\begin{bmatrix} 0 & 0 & \tilde{e}_{31} \\ 0 & 0 & \tilde{e}_{32} \\ 0 & 0 & 0 \end{bmatrix}}_{\mathbf{C}_e^b} \underbrace{\begin{Bmatrix} 0 \\ 0 \\ E_z \end{Bmatrix}}_{\mathbf{E}^b} = \mathbf{C}^b\boldsymbol{\varepsilon}^b - \mathbf{C}_e^b\mathbf{E}^b \\ &\underbrace{\begin{Bmatrix} \sigma_{xz} \\ \sigma_{yz} \end{Bmatrix}}_{\boldsymbol{\tau}^s} = \underbrace{\begin{bmatrix} \tilde{C}_{55} & 0 \\ 0 & \tilde{C}_{44} \end{bmatrix}}_{\mathbf{C}^s} \underbrace{\begin{Bmatrix} \gamma_{xz} \\ \gamma_{yz} \end{Bmatrix}}_{\boldsymbol{\gamma}} - \underbrace{\begin{bmatrix} \tilde{e}_{15} & 0 \\ 0 & \tilde{e}_{24} \end{bmatrix}}_{\mathbf{C}_e^s} \underbrace{\begin{Bmatrix} E_x \\ E_y \end{Bmatrix}}_{\mathbf{E}^s} = \mathbf{C}^s\boldsymbol{\gamma} - \mathbf{C}_c^s\mathbf{E}^s \\ &\underbrace{\begin{Bmatrix} D_x \\ D_y \end{Bmatrix}}_{\mathbf{D}^p} = \begin{bmatrix} \tilde{e}_{15} & 0 \\ 0 & \tilde{e}_{24} \end{bmatrix} \begin{Bmatrix} \gamma_{xz} \\ \gamma_{yz} \end{Bmatrix} + \underbrace{\begin{bmatrix} \tilde{k}_{11} & 0 \\ 0 & \tilde{k}_{22} \end{bmatrix}}_{\mathbf{C}_k^s} \begin{Bmatrix} E_x \\ E_y \end{Bmatrix} = \mathbf{C}_e^s\boldsymbol{\gamma} + \mathbf{C}_k^s\mathbf{E}^s \\ &D_z = \tilde{e}_{31}\varepsilon_x + \tilde{e}_{32}\varepsilon_y + \tilde{k}_{33}E_z \end{aligned} \tag{20}$$

where

$$\begin{aligned} &\tilde{C}_{11} = C_{11} - \frac{C_{13}^2}{C_{33}};\; \tilde{C}_{12} = C_{12} - \frac{C_{13}^2}{C_{33}};\; \tilde{C}_{66} = C_{66} \\ &\tilde{C}_{55} = C_{55};\; \tilde{C}_{44} = C_{44} \\ &\tilde{e}_{31} = e_{31} - \frac{e_{13}e_{33}}{C_{33}};\; \tilde{e}_{15} = e_{15};\; \tilde{k}_{11} = k_{11} \\ &\tilde{k}_{33} = k_{33} + \frac{e_{33}^2}{C_{33}} \\ &\varepsilon_x = \varepsilon_{1x} + z\varepsilon_{2x} + f(z)\varepsilon_{3x} \\ &\varepsilon_y = \varepsilon_{1y} + z\varepsilon_{2y} + f(z)\varepsilon_{3y} \end{aligned} \tag{21}$$

in which C_{11}, C_{12}, C_{33}, C_{66}, e_{31}, e_{33}, k_{31}, k_{33} are material constants defined in Eq. (1) or Eq. (2) and

$$\varepsilon_{1x} = u_{0,x} \;;\; \varepsilon_{2x} = -w_{,xx} \;;\; \varepsilon_{3x} = \beta_{x,x}$$
$$\varepsilon_{1y} = v_{0,y} \;;\; \varepsilon_{2y} = -w_{,yy} \;;\; \varepsilon_{3y} = \beta_{y,y} \tag{22}$$

The virtual strain energy is formulated by inserting Eqs. (16) and (20) into Eq. (14)

$$\begin{aligned}\delta U = &\int_\Omega \left(\left(\delta\bar{\boldsymbol{\varepsilon}}^b\right)^T \bar{\mathbf{C}}^b \bar{\boldsymbol{\varepsilon}}^b - \left(\delta\bar{\boldsymbol{\varepsilon}}^b\right)^T \bar{\mathbf{C}}_e^b \bar{\mathbf{E}}^b \right) \mathrm{d}\Omega \\ &+ \int_\Omega \left(\left(\delta\boldsymbol{\varepsilon}_s\right)^T \bar{\mathbf{C}}^s \boldsymbol{\varepsilon}_s - \left(\delta\boldsymbol{\varepsilon}_s\right)^T \bar{\mathbf{C}}_e^s \bar{\mathbf{E}}^s \right) \mathrm{d}\Omega \\ &- \int_\Omega \left(\left(\delta\bar{\mathbf{E}}^s\right)^T \bar{\mathbf{C}}_e^s \boldsymbol{\varepsilon}_s + \left(\delta\bar{\mathbf{E}}^s\right)^T \bar{\mathbf{C}}_k^s \bar{\mathbf{E}}^s \right) \mathrm{d}\Omega \\ &- \int_\Omega \left(\delta\bar{E}_z\right)^T \left(\bar{\mathbf{C}}_{e31} \bar{\boldsymbol{\varepsilon}}_x + \bar{\mathbf{C}}_{e32} \bar{\boldsymbol{\varepsilon}}_y + \bar{C}_{k33} \bar{E}_z \right) \mathrm{d}\Omega \end{aligned} \tag{23}$$

where

$$\bar{\boldsymbol{\varepsilon}}^b = \begin{bmatrix} \boldsymbol{\varepsilon}_1 \\ \boldsymbol{\varepsilon}_2 \\ \boldsymbol{\varepsilon}_3 \end{bmatrix}; \bar{\boldsymbol{\varepsilon}}_x = \begin{bmatrix} \varepsilon_{1x} \\ \varepsilon_{2x} \\ \varepsilon_{3x} \end{bmatrix}; \bar{\boldsymbol{\varepsilon}}_y = \begin{bmatrix} \varepsilon_{1y} \\ \varepsilon_{2y} \\ \varepsilon_{3y} \end{bmatrix};$$
$$\bar{\mathbf{C}}^b = \begin{bmatrix} \mathbf{A}^b & \mathbf{B}^b & \mathbf{E}^b \\ \mathbf{B}^b & \mathbf{D}^b & \mathbf{F}^b \\ \mathbf{E}^b & \mathbf{F}^b & \mathbf{H}^b \end{bmatrix}; \bar{\mathbf{E}}^b = -\begin{bmatrix} 0 \\ 0 \\ \phi \end{bmatrix}; \bar{\mathbf{E}}^s = -\begin{bmatrix} \phi_{,x} \\ \phi_{,y} \end{bmatrix};$$
$$\left(\mathbf{A}^b, \mathbf{B}^b, \mathbf{D}^b, \mathbf{E}^b, \mathbf{F}^b, \mathbf{H}^b\right) = \int_{-h/2}^{h/2} \left(1, z, z^2, f(z), zf(z), f^2(z)\right) \mathbf{C}^b \mathrm{d}z$$
$$\bar{\mathbf{C}}_e^b = \left[\bar{\mathbf{C}}_e^{b1} \;\; \bar{\mathbf{C}}_e^{b2} \;\; \bar{\mathbf{C}}_e^{b3} \right];$$
$$\left(\bar{\mathbf{C}}_e^{b1}, \bar{\mathbf{C}}_e^{b2}, \bar{\mathbf{C}}_e^{b3}\right) = \int_{-h/2}^{h/2} \left(g'(z), zg'(z), f(z)g'(z)\right) \mathbf{C}_e^b \mathrm{d}z;$$
$$\bar{\mathbf{C}}^s = \int_{-h/2}^{h/2} \left(f'(z)\right)^2 \mathbf{C}^s \mathrm{d}z;$$
$$\bar{\mathbf{C}}_e^s = \int_{-h/2}^{h/2} g(z) \left(f'(z)\right)^2 \mathbf{C}_e^s \mathrm{d}z; \;\; \bar{\mathbf{C}}_k^s = \int_{-h/2}^{h/2} g(z) \mathbf{C}_k^s \mathrm{d}z;$$
$$\bar{\mathbf{C}}_{e31} = \left[\bar{\mathbf{C}}_{e31}^1 \;\; \bar{\mathbf{C}}_{e31}^2 \;\; \bar{\mathbf{C}}_{e31}^3 \right];$$
$$\left(\bar{\mathbf{C}}_{e31}^1, \bar{\mathbf{C}}_{e31}^2, \bar{\mathbf{C}}_{e31}^3\right) = \int_{-h/2}^{h/2} \left(g'(z), zg'(z), f(z)g'(z)\right) \tilde{e}_{31} \mathrm{d}z;$$
$$\bar{\mathbf{C}}_{e32} = \left[\bar{\mathbf{C}}_{e32}^1 \;\; \bar{\mathbf{C}}_{e32}^2 \;\; \bar{\mathbf{C}}_{e32}^3 \right];$$
$$\left(\bar{\mathbf{C}}_{e32}^1, \bar{\mathbf{C}}_{e32}^2, \bar{\mathbf{C}}_{e32}^3\right) = \int_{-h/2}^{h/2} \left(g'(z), zg'(z), f(z)g'(z)\right) \tilde{e}_{32} \mathrm{d}z;$$
$$\bar{C}_{k33} = \int_{-h/2}^{h/2} \left(g'(z)\right)^2 \tilde{k}_{33} \mathrm{d}z \tag{24}$$

Similarly, the virtual kinetic energy is described as

$$\delta K = \int_\Omega \left(1 - \lambda\nabla^2\right) (\delta\mathbf{u})^T \mathbf{I}_m \ddot{\mathbf{u}} \mathrm{d}\Omega \tag{25}$$

where

$$\mathbf{u} = \begin{Bmatrix} \mathbf{u}^1 \\ \mathbf{u}^2 \\ \mathbf{u}^3 \end{Bmatrix}; \mathbf{u}^1 = \begin{Bmatrix} u_0 \\ v_0 \\ w \end{Bmatrix}; \; \mathbf{u}^2 = -\begin{Bmatrix} w_{0,x} \\ w_{0,y} \\ 0 \end{Bmatrix}$$
$$\mathbf{u}^3 = \begin{Bmatrix} \beta_x \\ \beta_y \\ 0 \end{Bmatrix}; \; \mathbf{I}_m = \begin{bmatrix} \mathbf{I}_1 & \mathbf{I}_2 & \mathbf{I}_4 \\ \mathbf{I}_2 & \mathbf{I}_3 & \mathbf{I}_5 \\ \mathbf{I}_4 & \mathbf{I}_5 & \mathbf{I}_6 \end{bmatrix} \tag{26}$$

in which

$$\left(\mathbf{I}_1, \mathbf{I}_2, \mathbf{I}_3, \mathbf{I}_4, \mathbf{I}_5, \mathbf{I}_6\right) = \int_{-h/2}^{h/2} \rho(z) \left(1, z, z^2, f(z), zf(z), f^2(z)\right) \begin{bmatrix} 1 & 0 & 0 \\ 0 & 1 & 0 \\ 0 & 0 & 1 \end{bmatrix} \mathrm{d}z \tag{27}$$

The virtual external work subjected to an external transverse load (f) can be expressed as follows

$$\delta W = \int_\Omega \left(1 - \lambda\nabla^2\right) \delta w^T f \mathrm{d}\Omega \tag{28}$$

In this research, the FGPP nanoplate is additionally considered the pre-buckling in-plane load by the electrical field, the variation of potential energy is expressed as

$$\delta V = -h \int_\Omega \left(1 - \lambda\nabla^2\right) \delta \begin{Bmatrix} w_{0,x} \\ w_{0,y} \end{Bmatrix}^{\mathrm{T}} \begin{bmatrix} N_x^0 & 0 \\ 0 & N_y^0 \end{bmatrix} \begin{Bmatrix} w_{0,x} \\ w_{0,y} \end{Bmatrix} \mathrm{d}\Omega \text{ or}$$
$$\delta V = -h \int_\Omega \left(1 - \lambda\nabla^2\right) \delta (\mathbf{B}^g)^{\mathrm{T}} \begin{bmatrix} N_x^0 & 0 \\ 0 & N_y^0 \end{bmatrix} \mathbf{B}^g \mathrm{d}\Omega \tag{29}$$

where $N_x^0 = N_x^{mech} + N_x^{elec}$ and $N_y^0 = N_y^{mech} + N_y^{elec}$; in which N_x^{mech} and N_y^{mech} are in-plane mechanical loads, whereas electrical components are $N_x^{elec} = N_y^{elec} = 2e_{31}^p V_0$.

Finally, Eq. (13) can be rewritten by

$$\delta U + \delta K - \delta W - \delta V = 0 \tag{30}$$

3.3 NURBS formulation for the FGPP nanoplate

The displacement field of the FGPP nanoplate is defined as

$$\mathbf{u}^h = \sum_{I=1}^{m\times n} \begin{bmatrix} R_I & 0 & 0 & 0 & 0 \\ 0 & R_I & 0 & 0 & 0 \\ 0 & 0 & R_I & 0 & 0 \\ 0 & 0 & 0 & R_I & 0 \\ 0 & 0 & 0 & 0 & R_I \end{bmatrix} \begin{Bmatrix} u_{0I} \\ v_{0I} \\ w_{0I} \\ \beta_{xI} \\ \beta_{yI} \end{Bmatrix} = \sum_{I=1}^{m\times n} \mathbf{R}_I \mathbf{d}_I \tag{31}$$

where $m\times n$ is the number of basis functions,R_I is a matrix of NURBS basis function (Hughes et al. 2005), $\mathbf{d}_I = \{ u_{0I}\ v_{0I}\ w_{0I}\ \beta_{xI}\ \beta_{yI} \}^T$ are degrees of freedom of the control point I.

Substituting Eq. (31) into Eq. (17) to form of Eq. (32):

$$\begin{aligned} \bar{\boldsymbol{\varepsilon}}^b &= \{ \boldsymbol{\varepsilon}_1\ \boldsymbol{\varepsilon}_2\ \boldsymbol{\varepsilon}_3 \}^T = \sum_{I=1}^{m\times n} \{ \mathbf{B}_I^1\ \mathbf{B}_I^2\ \mathbf{B}_I^3 \}^T \mathbf{d}_I \\ &= \sum_{I=1}^{m\times n} \mathbf{B}_I^b \mathbf{d}_I ; \bar{\boldsymbol{\varepsilon}}_s = \sum_{I=1}^{m\times n} \mathbf{B}_I^s \mathbf{d}_I \end{aligned} \tag{32}$$

where

$$\begin{aligned} \mathbf{B}_I^1 &= \begin{bmatrix} R_{I,x} & 0 & 0\ 0\ 0 \\ 0 & R_{I,y} & 0\ 0\ 0 \\ R_{I,y} & R_{I,x} & 0\ 0\ 0 \end{bmatrix}; \mathbf{B}_I^2 = -\begin{bmatrix} 0\ 0 & R_{I,xx} & 0\ 0 \\ 0\ 0 & R_{I,yy} & 0\ 0 \\ 0\ 0 & 2R_{I,xy} & 0\ 0 \end{bmatrix} \\ \mathbf{B}_I^3 &= \begin{bmatrix} 0\ 0\ 0 & R_{I,x} & 0 \\ 0\ 0\ 0 & 0 & R_{I,y} \\ 0\ 0\ 0 & R_{I,y} & R_{I,x} \end{bmatrix}; \mathbf{B}_I^s = \begin{bmatrix} 0\ 0\ 0 & R_I & 0 \\ 0\ 0\ 0 & 0 & R_I \end{bmatrix} \end{aligned} \tag{33}$$

Substituting Eq. (31) into Eq. (26) to form of Eq. (34):

$$\mathbf{u} = \{ \mathbf{u}^1\ \mathbf{u}^2\ \mathbf{u}^3 \}^T = \sum_{I=1}^{m\times n} \{ \mathbf{N}_I^1\ \mathbf{N}_I^2\ \mathbf{N}_I^3 \}^T \mathbf{q}_I = \sum_{I=1}^{m\times n} \overline{\mathbf{N}}_I \mathbf{q}_I \tag{34}$$

where

$$\mathbf{N}_I^1 = \begin{bmatrix} R_I & 0 & 0\ 0\ 0 \\ 0 & R_I & 0\ 0\ 0 \\ 0 & 0 & R_I\ 0\ 0 \end{bmatrix}; \mathbf{N}_I^2 = -\begin{bmatrix} 0\ 0 & R_{I,x} & 0\ 0 \\ 0\ 0 & R_{I,y} & 0\ 0 \\ 0\ 0 & 0 & 0\ 0 \end{bmatrix}; \mathbf{N}_I^3 = \begin{bmatrix} 0\ 0\ 0 & R_I & 0 \\ 0\ 0\ 0 & 0 & R_I \\ 0\ 0\ 0 & 0 & 0 \end{bmatrix} \tag{35}$$

Substituting Eq. (31) into Eq. (29),$\mathbf{B}^g$ can be expressed as

$$\mathbf{B}^g = \begin{bmatrix} 0\ 0 & R_{I,x} & 0\ 0 \\ 0\ 0 & R_{I,y} & 0\ 0 \end{bmatrix} \tag{36}$$

The electric potential can also be approximated using a NURBS basis function as follows

$$\phi = \sum_{I=1}^{m\times n} R_I \phi_I \tag{37}$$

where ϕ_I is the degree of freedom of the electric potential at the control point I.

Substituting Eqs. (31), (37) into Eqs. (22), (24), we have

$$\begin{aligned} &\bar{\mathbf{E}}^b = \sum_{I=1}^{m\times n} \mathbf{B}_{\phi I}^b \phi_I ;\ \bar{\mathbf{E}}^s = \sum_{I=1}^{m\times n} \mathbf{B}_{\phi I}^s \phi_I ;\ \bar{E}_z = \sum_{I=1}^{m\times n} \mathbf{B}_{zI} \phi_I \\ &\bar{\boldsymbol{\varepsilon}}_x = \sum_{I=1}^{m\times n} \mathbf{B}_{xI} \mathbf{d}_I ;\ \varepsilon_{1x} = \sum_{I=1}^{m\times n} \mathbf{B}_{xI}^1 \mathbf{d}_I ; \varepsilon_{3x} = \sum_{I=1}^{m\times n} \mathbf{B}_{xI}^3 \mathbf{d}_I \\ &\varepsilon_{2x} = \sum_{I=1}^{m\times n} \mathbf{B}_{xI}^2 \mathbf{d}_I ;\ \bar{\boldsymbol{\varepsilon}}_y = \sum_{I=1}^{m\times n} \mathbf{B}_{yI} \mathbf{d}_I ; \varepsilon_{1y} = \sum_{I=1}^{m\times n} \mathbf{B}_{yI}^1 \mathbf{d}_I \\ &\varepsilon_{2y} = \sum_{I=1}^{m\times n} \mathbf{B}_{yI}^2 \mathbf{d}_I ; \varepsilon_{3y} = \sum_{I=1}^{m\times n} \mathbf{B}_{yI}^3 \mathbf{d}_I \end{aligned} \tag{38}$$

where

$$\begin{aligned} &\mathbf{B}_{\phi I}^b = -\sum_{I=1}^{m\times n} \begin{bmatrix} 0 \\ 0 \\ R_I \end{bmatrix};\ \mathbf{B}_{\phi I}^s = -\sum_{I=1}^{m\times n} \begin{bmatrix} R_{I,x} \\ R_{I,y} \end{bmatrix} \\ &\mathbf{B}_{zI} = -\sum_{I=1}^{m\times n} R_I ;\ \mathbf{B}_{xI} = \begin{bmatrix} \mathbf{B}_{xI}^1 \\ \mathbf{B}_{xI}^2 \\ \mathbf{B}_{xI}^3 \end{bmatrix};\ \mathbf{B}_{yI} = \begin{bmatrix} \mathbf{B}_{yI}^1 \\ \mathbf{B}_{yI}^2 \\ \mathbf{B}_{yI}^3 \end{bmatrix} \\ &\mathbf{B}_{xI}^1 = \sum_{I=1}^{m\times n} \begin{bmatrix} R_{I,x}\ 0\ 0\ 0\ 0 \end{bmatrix} \\ &\mathbf{B}_{xI}^2 = -\sum_{I=1}^{m\times n} \begin{bmatrix} 0\ 0\ R_{I,xx}\ 0\ 0 \end{bmatrix}; \mathbf{B}_{xI}^3 = \sum_{I=1}^{m\times n} \begin{bmatrix} 0\ 0\ 0\ R_{I,x}\ 0 \end{bmatrix} \\ &\mathbf{B}_{yI}^1 = \sum_{I=1}^{m\times n} \begin{bmatrix} 0\ R_{I,y}\ 0\ 0\ 0 \end{bmatrix} \\ &\mathbf{B}_{yI}^2 = -\sum_{I=1}^{m\times n} \begin{bmatrix} 0\ 0\ R_{I,yy}\ 0\ 0 \end{bmatrix}; \mathbf{B}_{yI}^3 = \sum_{I=1}^{m\times n} \begin{bmatrix} 0\ 0\ 0\ 0\ R_{I,y} \end{bmatrix} \end{aligned} \tag{39}$$

The weak form of the FGPP nanoplates can be taken by substituting Eqs. (32)-(36), (38)-(39) into Eq. (30)

Table 1 Material properties of piezoelectric

Properties	PZT-4	PZT-5H
$c_{11}=c_{22}$ (GPa)	139	126
c_{12}	77.8	79.1
c_{13}	74	83.9
c_{33}	115	117
c_{55}	25.6	23
c_{66}	30.6	23.5
e_{31} (Cm^{-2})	−5.2	−6.5
e_{33}	15.1	23.3
e_{15}	12.7	17
k_{11} ($\mathrm{C}^2\mathrm{m}^{-2}\mathrm{N}^{-1}$)	6.46×10^{-9}	15.05×10^{-9}
k_{33}	5.62×10^{-9}	13.02×10^{-9}
ρ(kg/m^3)	7500	7500

$$\begin{bmatrix}\mathbf{M} & 0\\ \mathbf{0} & 0\end{bmatrix}\begin{bmatrix}\ddot{\mathbf{d}}\\ \ddot{\phi}\end{bmatrix}+\begin{bmatrix}\mathbf{K}_{uu} & \mathbf{K}_{u\phi}\\ \mathbf{K}_{\phi u} & \mathbf{K}_{\phi\phi}\end{bmatrix}\begin{bmatrix}\mathbf{d}\\ \phi\end{bmatrix}=\begin{bmatrix}\mathbf{f}\\ \mathbf{0}\end{bmatrix} \tag{40}$$

where

$$\begin{aligned}&\mathbf{K}_{uu}=\mathbf{K}_1+\mathbf{K}_3-\mathbf{K}_w\,;\quad \mathbf{K}_{u\phi}=-\left(\mathbf{K}_5+\mathbf{K}_{71}+\mathbf{K}_{72}\right)\\ &\mathbf{K}_{\phi u}=-\left(\mathbf{K}_2+\mathbf{K}_4\right);\mathbf{K}_{\phi\phi}=-\left(\mathbf{K}_6+\mathbf{K}_{73}\right)\\ &\mathbf{M}=\int_\Omega\left(1-\lambda\nabla^2\right)\overline{\mathbf{N}}^T\mathbf{I}_m\overline{\mathbf{N}}\mathrm{d}\Omega\,;\ \mathbf{f}=\int_\Omega\left(\mathbf{B}^w-\lambda\nabla^2\mathbf{B}^w\right)f\mathrm{d}\Omega\end{aligned} \tag{41}$$

in which

$$\begin{aligned}&\mathbf{K}_1=\int_\Omega\left(\mathbf{B}^b\right)^T\overline{\mathbf{C}}^b\mathbf{B}^b\mathrm{d}\Omega\,;\ \mathbf{K}_2=\int_\Omega\left(\mathbf{B}_\phi^b\right)^T\overline{\mathbf{C}}_e^b\mathbf{B}^b\mathrm{d}\Omega\,;\ \ \mathbf{K}_3=\int_\Omega(\mathbf{B}^s)^T\overline{\mathbf{C}}^s\mathbf{B}^s\mathrm{d}\Omega\\ &\mathbf{K}_4=\int_\Omega\left(\mathbf{B}_\phi^s\right)^T\overline{\mathbf{C}}_e^s\mathbf{B}^s\mathrm{d}\Omega\,;\ \mathbf{K}_5=\int_\Omega(\mathbf{B}^s)^T\overline{\mathbf{C}}_e^s\mathbf{B}_\phi^s\mathrm{d}\Omega\,;\ \mathbf{K}_6=\int_\Omega\left(\mathbf{B}_\phi^s\right)^T\overline{\mathbf{C}}_k^s\mathbf{B}_\phi^s\mathrm{d}\Omega\\ &\mathbf{K}_{71}=\int_\Omega\left(\mathbf{B}_x\right)^T\overline{\mathbf{C}}_{e31}\mathbf{B}_z\mathrm{d}\Omega\,;\ \mathbf{K}_{72}=\int_\Omega\left(\mathbf{B}_y\right)^T\overline{\mathbf{C}}_{e32}\mathbf{B}_z\mathrm{d}\Omega\,;\ \mathbf{K}_{73}=\int_\Omega\left(\mathbf{B}_z\right)^T\overline{C}_{k33}\mathbf{B}_z\mathrm{d}\Omega\\ &\mathbf{K}_w=\int_\Omega\left(1-\lambda\nabla^2\right)(\mathbf{B}^g)^T\begin{bmatrix}N_x^0 & 0\\ 0 & N_y^0\end{bmatrix}\mathbf{B}^g\mathrm{d}\Omega;\mathbf{B}^w=\begin{bmatrix}0 & 0 & R_I & 0 & 0\end{bmatrix}^T\end{aligned} \tag{42}$$

Substituting the second line of Eq. (40) into the first line, we have a shortened form as follows

$$\mathbf{M}\ddot{\mathbf{d}}+\left(\mathbf{K}_{uu}-\mathbf{K}_{u\phi}\mathbf{K}_{\phi\phi}^{-1}\mathbf{K}_{\phi u}\right)\mathbf{d}=\mathbf{f} \tag{43}$$

The principal equation of the free vibration problem is provided as follows

$$\left(\mathbf{K}-\omega^2\mathbf{M}\right)\mathbf{d}=\mathbf{0} \tag{44}$$

Table 2 The lowest non-dimensional natural frequency of the SSSS FGPP-II nanoplate with $\alpha=0.2$, $\lambda=0$, $a/h=100$

V_0 [V]	Methods	$n=0.2$	$n=1$	$n=5$
0	Ref. (Barati et al. 2017)	6.2072	5.9746	5.8028
	Present	6.2076	5.9749	5.8032
500	Ref. (Barati et al. 2017)	6.0324	5.7886	5.6076
	Present	6.0329	5.7890	5.6079

In which the global stiffness matrix $\mathbf{K}$ is taken as

$$\mathbf{K}=\mathbf{K}_{uu}-\mathbf{K}_{u\phi}\mathbf{K}_{\phi\phi}^{-1}\mathbf{K}_{\phi u} \tag{45}$$

4 Numerical examples

This section verifies the current findings and introduces new results. Table 1 outlines the material properties of piezoelectric. A mesh composed of 11×11 cubic Non-Uniform Rational B-Splines elements is utilized. The boundary conditions for each edge can either be clamped (C), free (F), or simply supported (S).

4.1 Square nanoplates

We now consider a square nanoplate with a length of a and thickness of h. The non-dimensional natural frequency $\tilde{\omega}=\omega a^2/h\sqrt{\left(\rho/c_{11}\right)_{PZT-4}}$ is being used for analysis purposes. Table 2 shows the first non-dimensional frequency of the entirely simply supported (SSSS) FGPP nanoplate for different values of input voltage and power law index. The results

Table 3 The effect of the nonlocal parameter on the first natural frequency of a CCCC FGPP nanoplate with $V_0=0$, $a/h=100$

α	λ	FGPP-I				FGPP-II			
		$n=0.1$	$n=1$	$n=2$	$n=6$	$n=0.1$	$n=1$	$n=2$	$n=6$
0	0	9.5274	9.1032	8.9956	8.8594	9.5274	9.1032	8.9956	8.8594
	1	1.8794	1.7957	1.7745	1.7476	1.8794	1.7957	1.7745	1.7476
	2	1.3416	1.2818	1.2667	1.2475	1.3416	1.2818	1.2667	1.2475
	3	1.0989	1.0500	1.0376	1.0218	1.0989	1.0500	1.0376	1.0218
	4	0.9532	0.9108	0.9000	0.8864	0.9532	0.9108	0.9000	0.8864
0.1	0	9.5783	9.1012	8.9815	8.8312	9.6641	9.2206	9.1085	8.9670
	1	1.8894	1.7953	1.7717	1.7420	1.9064	1.8189	1.7967	1.7688
	2	1.3488	1.2816	1.2647	1.2435	1.3608	1.2984	1.2826	1.2627
	3	1.1048	1.0497	1.0359	1.0186	1.1147	1.0635	1.0506	1.0343
	4	0.9583	0.9106	0.8986	0.8835	0.9669	0.9225	0.9113	0.8971
0.2	0	9.6443	9.0984	8.9634	8.7957	9.8140	9.3492	9.2321	9.0851
	1	1.9024	1.7947	1.7681	1.7350	1.9359	1.8442	1.8212	1.7921
	2	1.3580	1.2812	1.2622	1.2385	1.3820	1.3165	1.3000	1.2793
	3	1.1124	1.0494	1.0338	1.0145	1.1320	1.0784	1.0649	1.0479
	4	0.9649	0.9103	0.8968	0.8800	0.9819	0.9354	0.9237	0.9090
0.3	0	9.7336	9.0943	8.9396	8.7498	9.9790	9.4907	9.3682	9.2150
	1	1.9201	1.7939	1.7634	1.7260	1.9685	1.8722	1.8480	1.8178
	2	1.3706	1.2806	1.2588	1.2321	1.4052	1.3364	1.3192	1.2976
	3	1.1227	1.0489	1.0311	1.0092	1.1510	1.0947	1.0806	1.0629
	4	0.9738	0.9099	0.8944	0.8754	0.9984	0.9496	0.9373	0.9220

Table 4 The effect of external electric voltage on the first natural frequency of a SSSS FGPP-II nanoplate with $a/h=20$, $n=5$

α	λ	V_0 [V]						
		−500	−300	−100	0	100	300	500
0.1	1	1.0862	1.0816	1.0770	1.0747	1.0724	1.0677	1.0630
	2	0.7853	0.7789	0.7725	0.7692	0.7660	0.7594	0.7528
	3	0.6502	0.6425	0.6346	0.6307	0.6267	0.6187	0.6105
	4	0.5697	0.5609	0.5519	0.5473	0.5427	0.5334	0.5240
0.2	1	1.1000	1.0954	1.0908	1.0885	1.0862	1.0815	1.0768
	2	0.7951	0.7888	0.7824	0.7791	0.7759	0.7694	0.7628
	3	0.6582	0.6505	0.6427	0.6388	0.6348	0.6268	0.6187
	4	0.5767	0.5678	0.5589	0.5544	0.5498	0.5405	0.5311
0.3	1	1.1151	1.1105	1.1059	1.1036	1.1013	1.0967	1.0920
	2	0.8059	0.7996	0.7932	0.7900	0.7867	0.7802	0.7737
	3	0.6671	0.6594	0.6516	0.6477	0.6437	0.6358	0.6277
	4	0.5843	0.5755	0.5666	0.5621	0.5575	0.5483	0.5389

obtained in this research are consistent with those presented in Ref. (Barati et al. 2017) which used an analytical solution and a refined four-variable plate theory. However, the values obtained in our study are slightly larger than the reference values due to the use of different theories.

The following section investigates the effect of the nonlocal parameter on the first frequency of a fully clamped (CCCC) FGPP nanoplate, as shown in Table 3. The results indicate that the natural frequency of the plate decreases as the nonlocal parameter increases. Additionally, an increase in the power law exponent leads to a decrease in the

Table 5 The first six natural frequencies of a SSSS FGPP-I nanoplate with $a/h=100$, $\lambda=2$, $V_0=0$

α	n	Modes					
		1	2	3	4	5	6
0.1	0	0.8398	1.3371	1.3371	1.6935	1.8944	1.8944
	2	0.7750	1.2339	1.2339	1.5629	1.7482	1.7482
	4	0.7668	1.2208	1.2208	1.5464	1.7297	1.7297
	6	0.7620	1.2132	1.2132	1.5368	1.7189	1.7189
	8	0.7587	1.2078	1.2078	1.5300	1.7113	1.7113
	10	0.7561	1.2038	1.2038	1.5249	1.7056	1.7056
0.2	0	0.8480	1.3501	1.3501	1.7100	1.9129	1.9129
	2	0.7734	1.2314	1.2314	1.5597	1.7447	1.7447
	4	0.7643	1.2168	1.2168	1.5413	1.7240	1.7240
	6	0.7590	1.2083	1.2083	1.5306	1.7120	1.7120
	8	0.7552	1.2024	1.2024	1.5230	1.7036	1.7036
	10	0.7524	1.1979	1.1979	1.5174	1.6972	1.6972
0.3	0	0.8596	1.3686	1.3686	1.7334	1.9391	1.9391
	2	0.7714	1.2281	1.2281	1.5556	1.7400	1.7400
	4	0.7610	1.2116	1.2116	1.5347	1.7166	1.7166
	6	0.7550	1.2020	1.2020	1.5226	1.7031	1.7031
	8	0.7508	1.1953	1.1953	1.5141	1.6935	1.6935
	10	0.7476	1.1902	1.1902	1.5077	1.6864	1.6864

Table 6 The first natural frequency of a FGPP nanoplate with $\alpha = 0.3$, $n=3$, $a/h=50$

BCs	V_0 [V]	FGPP-I				FGPP-II			
		λ				λ			
		1	2	3	4	1	2	3	4
CCCC	−300	1.9105	1.4713	1.2872	1.1834	1.9852	1.5181	1.3210	1.2094
	0	1.7438	1.2448	1.0196	0.8844	1.8299	1.3062	1.0700	0.9281
	300	1.5593	0.9666	0.6500	0.4051	1.6601	1.0526	0.7379	0.5100
SSSS	−300	1.1725	0.9048	0.7919	0.7281	1.2187	0.9339	0.8130	0.7444
	0	1.0679	0.7644	0.6267	0.5439	1.1212	0.8025	0.658	0.5710
	300	0.9518	0.5914	0.3978	0.2474	1.0143	0.6448	0.4524	0.3127
CFCF	−300	1.7490	1.3607	1.1953	1.1016	1.8168	1.4033	1.2261	1.1251
	0	1.5942	1.1479	0.9430	0.8191	1.6727	1.2044	0.9894	0.8595
	300	1.4228	0.8869	0.5960	0.3712	1.515	0.9665	0.6776	0.4679
SCFS	−300	1.2996	1.0085	0.8836	0.8124	1.3509	1.0412	0.9074	0.8308
	0	1.1877	0.8563	0.7037	0.6115	1.2466	0.8988	0.7387	0.6418
	300	1.0633	0.6676	0.4519	0.2831	1.1322	0.7269	0.5129	0.3564

natural frequency. It is worth noting that the natural frequency of the FGPP-I nanoplate is smaller than that of the FGPP-II nanoplate. Table 4 presents the impact of the external electric voltage on the first natural frequency of a SSSS FGPP-II nanoplate. The results show that an increase in the external electric voltage results in a decrease in the frequency of the nanoplate.

In addition, Table 5 lists the first six natural frequencies of a SSSS FGPP-I nanoplate. The results show that the natural frequencies decrease as the power law exponent increases and increase as the

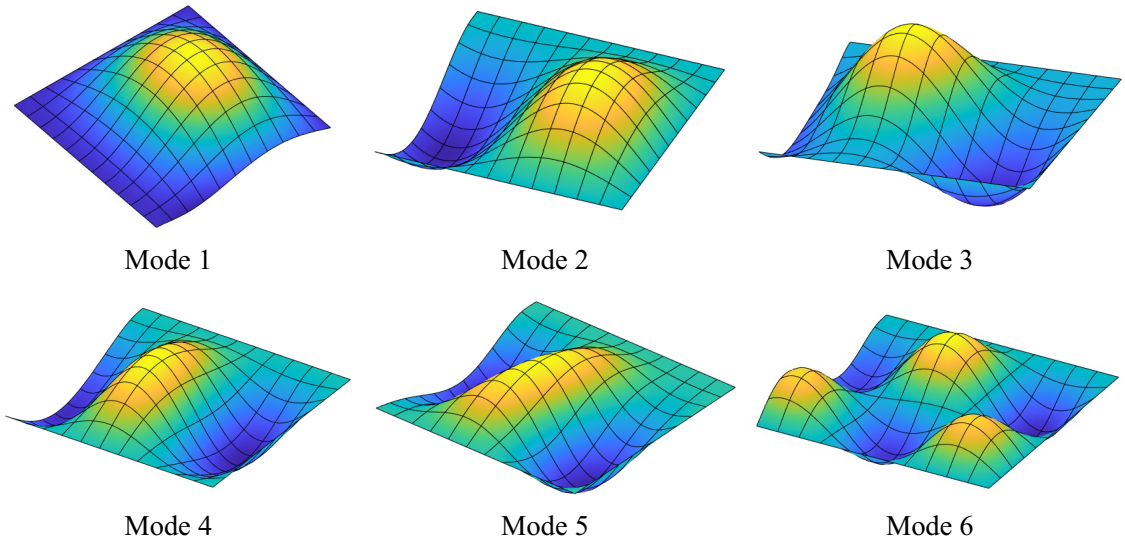

Fig. 2 The first six mode shapes of the SCFS FGPP-I nanoplate with $\alpha = 0.3$, $\lambda = 3$, $a/h = 50$, $n = 3$, $V_0 = 300$

Table 7 The first natural frequency of a simply supported circular FGPP nanoplate with $\alpha = 0.3$, $R/h = 20$

n	λ	FGPP-I			FGPP-II		
		$V_0 = -500$	$V_0 = 0$	$V_0 = 500$	$V_0 = -500$	$V_0 = 0$	$V_0 = 500$
0	1	2.2258	2.2119	2.1979	2.2623	2.2476	2.2327
	2	1.6437	1.6250	1.6061	1.6710	1.6512	1.6311
	3	1.3671	1.3447	1.3218	1.3902	1.3664	1.3421
	4	1.1981	1.1726	1.1463	1.2186	1.1915	1.1635
2	1	2.0117	1.9868	1.9616	2.1038	2.0804	2.0567
	2	1.4929	1.4596	1.4254	1.5597	1.5284	1.4962
	3	1.2477	1.2079	1.1664	1.3022	1.2648	1.2258
	4	1.0984	1.0533	1.0055	1.1454	1.1029	1.0579
10	1	1.9574	1.9282	1.8984	2.0597	2.0329	2.0057
	2	1.4556	1.4166	1.3761	1.5293	1.4935	1.4565
	3	1.2188	1.1722	1.1233	1.2787	1.2359	1.1911
	4	1.0751	1.0222	0.9658	1.1262	1.0777	1.0261
20	1	1.9381	1.9080	1.8772	2.0442	2.0167	1.9887
	2	1.4420	1.4017	1.3599	1.5183	1.4816	1.4436
	3	1.2081	1.1600	1.1093	1.2699	1.2261	1.1800
	4	1.0660	1.0115	0.9532	1.1189	1.0691	1.0161

porous volume fraction increases. The effect of different boundary conditions on the natural frequency of the nanoplate is presented in Table 6. As demonstrated in the table, the highest and lowest frequencies are obtained for the CCCC and SSSS nanoplates, respectively. Figure 2 illustrates the first six mode shapes of the SCFS FGPP-I square nanoplate.

Table 8 The effect of different boundary conditions on the first natural frequency of a circular FGPP nanoplate with $\alpha = 0.1$, $R/h = 20$, $n = 0.5$

BCs	V_0	FGPP-I				FGPP-II			
		λ				λ			
		1	2	3	4	1	2	3	4
Fully clamped	−500	3.7079	2.7248	2.2654	1.9869	3.7500	2.7554	2.2905	2.0087
	0	3.6782	2.6830	2.2144	1.9282	3.7206	2.7139	2.2399	1.9504
	500	3.6483	2.6406	2.1622	1.8678	3.6908	2.6718	2.1881	1.8904
Simply supported	−500	2.0734	1.5352	1.2802	1.1247	2.0974	1.5528	1.2947	1.1373
	0	2.0537	1.5088	1.2486	1.0887	2.0778	1.5265	1.2632	1.2632
	500	2.0337	1.4817	1.2158	1.0511	2.0579	1.4996	1.2307	1.0640

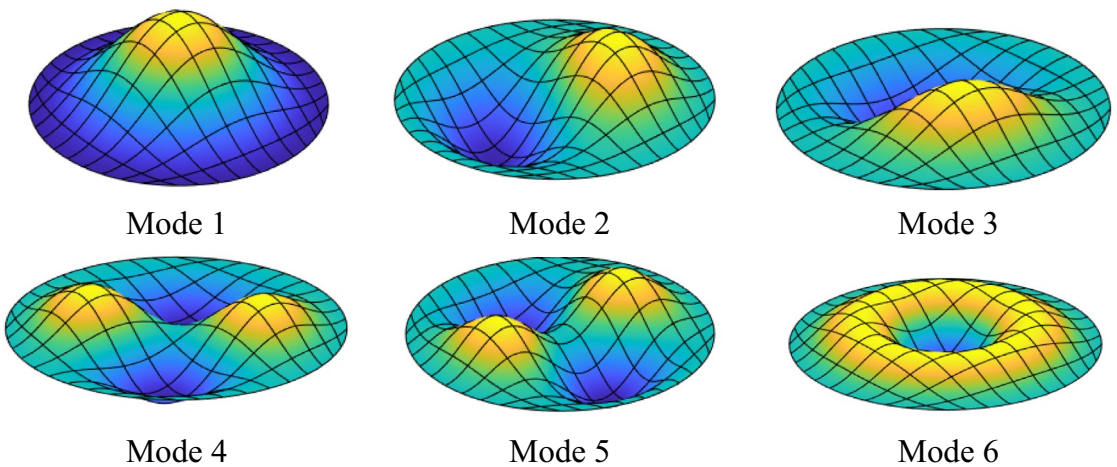

Fig. 3 The first six mode shapes of the fully clamped circular FGPP-I nanoplate with $\alpha = 0.1$, $\lambda = 4$, $R/h = 20$, $n = 0.5$, $V_0 = 500$

4.2 Circular nanoplates

A FGPP circular nanoplate with radius R and thickness h is considered in this section. The non-dimensional natural frequency $\tilde{\omega} = 4\omega R^2/h\sqrt{(\rho/c_{11})_{PZT-4}}$ is used. The effect of the nonlocal parameter and external electric voltage on the first natural frequency of the simply supported circular FGPP nanoplate is shown in Table 7. The finding is that the frequency decreases with increasing of the nonlocal parameter and external electric voltage, respectively.

Next, the influence of different boundary conditions on the first natural frequency of a circular FGPP nanoplate is shown in Table 8. Again, we can see that the natural frequency of the FGPP-I nanoplate is smaller than that of the FGPP-II nanoplate. And, the natural frequency of the nanoplates decreases with a rise of the nonlocal parameter and external electric voltage. Finally, the lowest six mode shapes of a fully clamped circular FGPP nanoplate are also plotted in Fig. 3.

5 Conclusions

This paper presented the size-dependent analysis of the functionally graded piezoelectric porous nanoplates using higher-order shear deformation theory, the nonlocal elasticity and isogeometric analysis. Material properties of the nanoplate made of two piezoelectric materials including PZT-4 and PZT-5H are performed by using the modified power-law function. Two porous distributions through the thickness direction are employed. The Eringen's nonlocal elasticity

is used to simulate the size-dependent effects. Based on the study results and the established formulations, some remarkable conclusions can be listed as follows:

- Isogeometric analysis of porous-dependent FG piezoelectric porous nanoplates is extended and developed in this study.
- The combination of the Eringen's nonlocal elasticity theory and IGA is a simply, suitable, effective and robust method to calculate and simulate behaviors of the FG piezoelectric porous nanoplates.
- The frequency of the nanoplates decreases with increasing of the nonlocal parameter and external electric voltage.
- The frequency of the FGPP-I nanoplate is smaller than that of the FGPP-II nanoplate.
- The frequency decreases and increases with increasing of the law exponent index and porous volume fraction factor, respectively.

Finally, these findings shed light on the behavior of smart functionally graded piezoelectric porous nanoplates and contribute to a more comprehensive understanding of the implications for future research in this field.

Acknowledgements This work belongs to the project grant No: T2022-136 funded by Ho Chi Minh City University of Technology and Education, Viet Nam.

Declarations

Conflict of interest The authors declare that they have no known competing financial interest or personal relationships that could have appeared to influence the work reported in this paper.

References

Barati, M.R., Shahverdi, H., Zenkour, A.M.: Electro-mechanical vibration of smart piezoelectric FG plates with porosities according to a refined four-variable theory. Mech. Adv. Mater. Struct. **24**(12), 987–998 (2017). https://doi.org/10.1080/15376494.2016.1196799

Behjat, B., Salehi, M., Sadighi, M., Armin, A., Abbasi, M.: Static, dynamic, and free vibration analysis of functionally graded piezoelectric panels using finite element method. J. Intell. Mater. Syst. Struct. **20**(13), 1635–1646 (2009). https://doi.org/10.1177/1045389X09104113

Brischetto, S., Carrera, E.: Refined 2D models for the analysis of functionally graded piezoelectric plates. J. Intell. Mater. Syst. Struct. **20**(15), 1783–1797 (2009). https://doi.org/10.1177/1045389X08098444

Chen, W., Ding, H.: On free vibration of a functionally graded piezoelectric rectangular plate. Acta Mech. **153**(3), 207–216 (2002)

Chen, W., Wang, L., Lu, Y.: Free vibrations of functionally graded piezoceramic hollow spheres with radial polarization. J. Sound Vib. **251**(1), 103–114 (2002). https://doi.org/10.1006/jsvi.2001.3973

Ebrahimi, F., Barati, M.R.: Buckling analysis of nonlocal third-order shear deformable functionally graded piezoelectric nanobeams embedded in elastic medium. J. Braz. Soc. Mech. Sci. Eng. **39**(3), 937–952 (2017). https://doi.org/10.1007/s40430-016-0551-5

Ebrahimi, F., Salari, E.: Size-dependent thermo-electrical buckling analysis of functionally graded piezoelectric nanobeams. Smart Mater. Struct. **24**(12), 125007 (2015). https://doi.org/10.1088/0964-1726/24/12/125007

Farzaneh Joubaneh, E., Mojahedin, A., Khorshidvand, A., Jabbari, M.: Thermal buckling analysis of porous circular plate with piezoelectric sensor-actuator layers under uniform thermal load. J. Sandwich Struct. Mater. **17**(1), 3–25 (2015). https://doi.org/10.1177/1099636214554172

Hughes, T.J., Cottrell, J.A., Bazilevs, Y.: Isogeometric analysis: CAD, finite elements, NURBS, exact geometry and mesh refinement. Comput. Methods Appl. Mech. Eng. **194**(39–41), 4135–4195 (2005). https://doi.org/10.1016/j.cma.2004.10.008

Hung, P., Phung-Van, P., Thai, C.H.: A refined isogeometric plate analysis of porous metal foam microplates using modified strain gradient theory. Compos. Struct. **289**, 115467 (2022). https://doi.org/10.1016/j.compstruct.2022.115467

Kiani, Y., Rezaei, M., Taheri, S., Eslami, M.: Thermo-electrical buckling of piezoelectric functionally graded material timoshenko beams. Int. J. Mech. Mater. Des. **7**(3), 185–197 (2011). https://doi.org/10.1007/s10999-011-9158-2

Li, Y., Xiao, T.: Free vibration of the one-dimensional piezoelectric quasicrystal microbeams based on modified couple stress theory. Appl. Math. Model. **96**, 733–750 (2021). https://doi.org/10.1016/j.apm.2021.03.028

Lu, P., Zhang, P., Lee, H., Wang, C., Reddy, J.: Non-local elastic plate theories. Proc. R. Soc. Math. Phys. Eng. Sci. **463**(2088), 3225–3240 (2007). https://doi.org/10.1098/rspa.2007.1903

Mehralian, F., Beni, Y.T., Ansari, R.: Size dependent buckling analysis of functionally graded piezoelectric cylindrical nanoshell. Compos. Struct. **152**, 45–61 (2016). https://doi.org/10.1016/j.compstruct.2016.05.024

Nguyen, L.B., Thai, C.H., Zenkour, A., Nguyen-Xuan, H.: An isogeometric Bézier finite element method for vibration analysis of functionally graded piezoelectric material porous plates. Int. J. Mech. Sci. **157**, 165–183 (2019). https://doi.org/10.1016/j.ijmecsci.2019.04.017

Phung-Van, P., Thai, C.H.: A novel size-dependent nonlocal strain gradient isogeometric model for functionally graded carbon nanotube-reinforced composite nanoplates. Eng. Comput. (2021). https://doi.org/10.1007/s00366-021-01353-3

Phung-Van, P., Ferreira, A., Nguyen-Xuan, H., Wahab, M.A.: An isogeometric approach for size-dependent geometrically nonlinear transient analysis of functionally graded nanoplates. Compos. B Eng. **118**, 125–134 (2017a). https://doi.org/10.1016/j.compositesb.2017.03.012

Phung-Van, P., Tran, L.V., Ferreira, A., Nguyen-Xuan, H., Abdel-Wahab, M.: Nonlinear transient isogeometric analysis of smart piezoelectric functionally graded material plates based on generalized shear deformation theory under thermo-electro-mechanical loads. Nonlinear Dyn. **87**(2), 879–894 (2017b). https://doi.org/10.1007/s11071-016-3085-6

Phung-Van, P., Thai, C.H., Abdel-Wahab, M., Nguyen-Xuan, H.: Optimal design of FG sandwich nanoplates using size-dependent isogeometric analysis. Mech. Mater. **142**, 103277 (2020). https://doi.org/10.1016/j.mechmat.2019.103277

Phung-Van, P., Ferreira, A., Thai, C.H.: Computational optimization for porosity-dependent isogeometric analysis of functionally graded sandwich nanoplates. Compos. Struct. **239**, 112029 (2020). https://doi.org/10.1016/j.compstruct.2020.112029

Phung-Van, P., Ferreira, A., Nguyen-Xuan, H., Thai, C.H.: Scale-dependent nonlocal strain gradient isogeometric analysis of metal foam nanoscale plates with various porosity distributions. Compos. Struct. **268**, 113949 (2021). https://doi.org/10.1016/j.compstruct.2021.113949

Su, Z., Jin, G., Ye, T.: Electro-mechanical vibration characteristics of functionally graded piezoelectric plates with general boundary conditions. Int. J. Mech. Sci. **138**, 42–53 (2018). https://doi.org/10.1016/j.ijmecsci.2018.01.040

Tadi, B.Y.: Size-dependent electromechanical bending, buckling, and free vibration analysis of functionally graded piezoelectric nanobeams. J. Intell. Mater. Syst. Struct. **27**(16), 2199–2215 (2016). https://doi.org/10.1177/1045389X15624798

Thai, C.H., Ferreira, A., Phung-Van, P.: Free vibration analysis of functionally graded anisotropic microplates using modified strain gradient theory. Eng. Anal. Boundary Elem. **117**, 284–298 (2020). https://doi.org/10.1016/j.enganabound.2020.05.003

Zenkour, A.M., Aljadani, M.H.: Porosity effect on thermal buckling behavior of actuated functionally graded piezoelectric nanoplates. Eur. J. Mech. -A/Solid. **78**, 103835 (2019). https://doi.org/10.1016/j.euromechsol.2019.103835

Zenkour, A.M., Aljadani, M.H.: Thermo-electrical buckling response of actuated functionally graded piezoelectric nanoscale plates. Results Phys. **13**, 102192 (2019). https://doi.org/10.1016/j.rinp.2019.102192

Zhang, T., Shi, Z., Spencer, B.: Vibration analysis of a functionally graded piezoelectric cylindrical actuator. Smart Mater. Struct.. **17**(2), 025018 (2008). https://doi.org/10.1088/0964-1726/17/2/025018

Zhong, Z., Shang, E.: Three-dimensional exact analysis of a simply supported functionally gradient piezoelectric plate. Int. J. Solids Struct. **40**(20), 5335–5352 (2003). https://doi.org/10.1016/S0020-7683(03)00288-9